Sedimentary basins of the Eastern Asia Arctic zone: new details on their structure revealed by decompensative gravity anomalies

Roman V. Sidorov[1], Mikhail K. Kaban[1,2,3], Anatoly A. Soloviev[1,3], Alexei G. Petrunin[1,2,3], Alexei D. Gvishiani[1,3], Alexei A. Oshchenko[1], Anton B. Popov[1], Roman I. Krasnoperov[1]

[1]Geophysical Center of the Russian Academy of Sciences (GC RAS), Moscow, Russia
[2]German Research Center for Geosciences (GFZ), Potsdam, Germany
[3]Schmidt Institute of Physics of the Earth of the Russian Academy of Sciences (IPE RAS), Moscow, Russia

Correspondence to: Roman V. Sidorov (r.sidorov@gcras.ru)

Abstract.

In the present study, structure of sedimentary basins in the Eastern Asia Arctic zone is analysed by employing the approach based on decompensative gravity anomalies. Two obtained models, differing in their initial conditions, provide thickness and density of sediments in the study area. They demonstrate essentially new details on the structure, shape and density of the sedimentary basins. Significant changes in the sedimentary thickness and the depocenter location have been found for the Anadyr basin in its continental part. Also, new details on the sedimentary thickness distribution have been revealed for the central part of the Penzhin and Pustorets basins, for the latter, the new location of the depocenter has been identified. The new model agrees well with the seismic data on the sedimentary thickness for the offshore part of the Chauna basin confirming that the method is robust. The most significant lateral redistribution of the thickness has been found for the Lower Cretaceous coal-bearing strata in the northern part of the Zyryanka basin, where the connection of two coal-bearing zones, that was not previously mapped, has been identified. Also, the new details on the sedimentary thickness distribution have been discovered for the Primorsk basin. Therefore, the new results substantially improve our knowledge about the region, since previous geological and geophysical studies were unsystematic, sparse and limited in depth. Thus, the implementation of the decompensative gravity anomalies approach provides a better understanding of the evolution of the sedimentary basins and the obtained results can be used for planning of future detailed studies in the area.

1 Introduction

In this study we analyze the structure of sedimentary basins in the North-Eastern part of Asia, including the Asia Arctic zone and the adjacent areas of the Arctic ocean, by employing the approach based on the decompensative gravity anomalies (Haeger and Kaban, 2019; Kaban et al., 2021a, b). This method is employed together with one of the most recent gravity field models EIGEN6-c4 (Förste et al, 2014).

The structure and density of sedimentary basins represent a natural record of the former tectonic activity. Therefore, knowledge on the sedimentary structure can provide a basis for understanding the history and formation of various

geological structures. This information can be used in various studies in geology and Earth history, geodynamics, oceanology, paleogeography etc. Furthermore, these results are important for numerous practical applications, particularly for mineral deposits prospecting and development of the necessary infrastructure, including pipelines and railways. This is the key issue for the economic development of such regions as the Asia Arctic zone.

Up to now, the North-Eastern part of Asia remains one of the least studied areas in the world, due to the inaccessibility of this territory, its rigorous climate, and low habitability. The systematic geographical and geological exploration of this region began only less than 100 years ago. One of the first effective scientific expeditions into the "middle of nowhere" was the expedition of S.V. Obruchev in 1926–1930, when one of the last mapped mountain ridges in Asia – the Chersky Ridge – was discovered. A lot of geological studies were conducted later in the North-Eastern Asia region, in particularly mineral prospecting (ore, carbohydrates, coal etc.) (e.g. Sitnikov 2017; Morozov, 2001). However, most of them were focused on surface geology, while the area is still poorly studied by geophysical (first of all, seismic) methods. Thus, the deep structure of many sedimentary basins remains unclear, and the information on their development is often based on very generalized and sometimes outdated hypotheses. Furthermore, for some particular areas within the Eastern Asia Arctic zone, like Chukotka, there exist contradicting hypotheses about their origin due to insufficient knowledge about their structure (Morozov, 2001). Therefore, detailed models of these structures obtained with modern geological and geophysical data and methods, can help to justify some of the suggested hypotheses.

The lithosphere in this region represents a complex combination of different structures that developed generally from the Jurassic to the Quaternary during several periods of intense tectonic activity and relatively quiet periods of sedimentation. Three large tectonic elements with different structural patterns and different history can be distinguished within the study area: the Verhkoyansk (Verkhoyansk-Chukotka) orogen, the Koryak orogen and the Okhotsk-Chukotka volcanogenic belt.

Gravity field is often used to study sedimentary basins because sediments normally have a large density contrast relative to surrounding consolidated rocks (e.g. Langenheim and Jachens, 1996; Jachens and Moring, 1990; Ebbing et al., 2007; Kaban et al., 2021a,b). On the other hand, the gravity data usually have complete and homogeneous data coverage, while seismic determinations are limited to seismic profiles or even single points. The recent satellite missions have provided data even for the continental areas not covered by terrestrial or airborne prospecting (e.g. Förste et al., 2014). Typically, the Bouguer or isostatic gravity anomalies are employed for studying sediments. The isostatic anomalies are considered more appropriate because they are refined to some extent from the effect of deep density variations (e.g. of the Moho undulations), which are dominated in the Bouguer anomalies (e.g. Simpson et al., 1986; Blakely 1995). Consequently, the isostatic gravity anomalies have been extensively used for these purposes (e.g. Jachens and Moring, 1990; Langenheim and Jachens, 1996; Ebbing et al., 2007).

However, this method works correctly only for small-scale basins like the Los Angeles basin (Langenheim and Jachens, 1996) or for narrow basins (e.g. in Nevada; Jachens and Moring, 1990). For larger basins, the gravity effect of sediments is significantly reduced due to isostatic compensation (e.g. Cordell et al., 1991). For wide basins (≈300–400 km and more) this reduction may even exceed one order of magnitude (Kaban et al., 2021a). Zorin et al. (1985) and Cordell et al. (1991)

suggested recovering the full effect of sediments by computing decompensative gravity anomalies. Afterwards, this method was successfully employed for studying the upper crust in many regions (Cordell et al., 1991; Hildenbrand et al., 1996; Zorin et al., 1993; Wilson et al., 2005). Recently, this approach has been improved to account for elastic deformations of the lithosphere via its effective elastic plate thickness (EET) (Kaban et al. 2017; Haeger and Kaban, 2019).

For implementing the method, we use the strategy, which was formulated in (Kaban et al., 2021b) for studying the southern part of the East European platform. In the first step, the isostatic anomalies of the gravity field are estimated. Then, we compute the decompensative correction for these anomalies and use it for improvement of the initial model of the sedimentary cover.

2 Study area

2.1 An overview of the geological and tectonic history

The study area represents a part of Northeastern Asia and spans from 135°E to 190°E and 65°N to 74°N. The topography and bathymetry of the region with main geological structures are shown in Fig. 1. Most of the continental area is represented by the Verkhoyansk orogen – a large system of mountain ridges that were formed during the Kimmerian time. The orogen is mostly dominated by the middle and late Paleozoic (Carboniferous and Permian) to Mesozoic (Triassic and Late Jurassic) terrigenous rocks accumulated in the passive margin conditions of the Siberian Platform and deformed then during the collision between the East Siberian and East Arctic continental lithospheric plates (Sitnikov and Sleptsova, 2020), and later – in the collision of the Pacific and the Chukotka plates. In the Late Mesozoic, continental magmatism led to the upwelling of granitic and granodiorite batholiths, forming the mountain ridges. The largest ridges forming the orogeny of this age in the studied region are the Chersky and Suntar-Khayata Ridges, as well as the Near-Kolyma uplifts (a part of the large Kolyma-Omolon superterrain). The eastern part of the region includes such large mountain ridges as the Kolyma Mountains, Chukotka Mountains, and Koryak Mountains (Anadyr-Koryak folded system). In the Late Cenozoic, new deformations occurred, complicating the Mezosoic tectonic structure of the orogen. In the central part of the region, the arched-block raised, while the northern parts of the region subsided, and a thin cover of the Cenozoic sediments was formed there. In the southern part of the sea shelf, the marine sediments accumulated.

The northern part of the territory is bounded by the Arctic Ocean Shelf of the Laptev Sea, East Siberian Sea, and Chukchi Sea.

Continental sedimentary basins of the studied territory formed as:

1. intermontane depressions of the Mesozoic basement;
2. basins filling new Cenozoic rifts (Laptev-Moma basin system);
3. continental margins of the sea shelf.

The Okhotsk-Chukotka volcanic belt (OCVB), located in the eastern part of the region, extends along the north coast of the Sea of Okhotsk for about 3000 km and then to the northeast in the Chukotsk Peninsula. Dashed line in Fig. 1 indicates

the OCVB continental borders. In the southwest, the Okhotsk segment of the belt is 1400 km long and is different in some ways from the Chukotka segment, which is 1600 km long. The belt is composed of subaerial volcanic rocks, in particularly of the rhyolites, andesites and basalts, forming the lava cover. The sedimentary rocks forming the OCVB structures are partly terrigenous, partly volcano-tuff-terrigenous, while the volcanoclastic rocks are much less abundant. Most of these rocks are of the late Early Cretaceous — Late Cretaceous age and younger. The eastern part of the Kolyma Mountains and southern part of the Chukotka mountains chiefly presented by the Cretaceous volcanogenic rocks related to the OCVB formation.

2.2 Sedimentary basins, their origin, and structure

Most of the sedimentary basins on the continental part are characterized by low thickness mainly due to a relatively short period of sedimentation in the passive continental margins or in the intermontane depressions (Sitnikov et al., 2017). The deepest sedimentary basins in the area are related to the grabens continuing to the Arctic shelf and formed on the Late Mesozoic and Cenozoic basement. In this study, we analyze relatively deep (more than 0.5 km) and most extended sedimentary basins in the continental part of the region and on the sea shelf. These basins are related to different stages of the geological evolution of the region and were formed during different periods (from the Middle and Late Mesozoic to the Cenozoic).

First of all, we consider the easternmost continental branches of the Laptev-Moma basin (LMB), which is a rift-related structure represented by the grabens appeared in the Cenozoic with the limnic deposits of the Oligocene — Middle Miocene. Over them, the alluvial-proluvial sediments of the Upper Miocene – Holocene were then accumulated. This structure is a part of the larger basin, which continues northward from the continent into the Laptev Sea shelf (the Southwest Laptev basin), which also includes the Lena River delta. In the continental part and the nearest shelf, the Shiroston and Ust'-Yana grabens can be also distinguished in the study region (Andieva, 2008).

The Zyryanka basin is an internal depression within the Kolyma massive. Geographically it comprises the valleys of the Indigirka and Kolyma Rivers. This large depression formed in the final stages of the Verkhoyansk Mesozoic orogeny. Some studies initially assumed that the Zyranka depression is a foredeep but not an intermontane depression (Koporulin, 1979). The sediments filling the depression are of the Upper Jurassic, Cretaceous, and Paleogenic to Quaternary ages (Clarke, 1988). The basement of the depression is irregular and exposed in several locations. In the post orogenic stage, during the Early Cretaceous, the strata of the continental limnic molasses (represented by sandstones, conglomerates, etc.) with thick coal beds was accumulated. The nearest Moma (Moma-Selennyakh) depression is located to the south from the Ilin'-Taas inversion uplift, separating it from the Zyryanka depression. Initially, these two depressions formed on the basis of the large Moma-Zyryanka rift system (Grachev et al., 1970), later a significant difference has been discovered in the sedimentary strata composing the upper part of the Moma depression (with higher metamorphism comparing to the Zyryanka depression). The Lower Cretaceous sediments in the Moma basin are represented only by Neocomian to Aptian strata in

isolated troughs with a maximum thickness of 3 km. The Cenozoic (Paleogenic to Quaternary) sedimentary thickness is relatively insignificant.

The Primorsk basin, according to its name given by Drachev et al. (2011), or the Lower Kolyma basin, according to Sitnikov and Sleptsova (2020), is located mainly in the East Siberian (or Lower Kolyma) lowland in the downstream of the Indigirka, Alazeya and Kolyma rivers, however, its northern part is located offshore on the Arctic Ocean shelf (the basin shape can be seen in Fig. 1). Its folded basement is represented by the Polousnensky folded structure on its western part and by the South Anyui suture in its eastern part. The Primorsk Lowland is covered by thick Neogene-Quaternary deposits, which complicate study of its structure. Therefore, the thickness of the sedimentary cover of this basin (of Meso-Cenozoic to Quaternary age) was differently determined in many existing studies.

The Tastakh (or Tas-Takh) basin is located west of the Primorsk basin and separated from it by the Khroma height. Pavlova (2020) suggests that the Tastakh basin is the marginal part the larger depression mostly located offshore. From the middle of the 1980s, it was studied by geological, gravimetric, and aeromagnetic surveys of various scales. The sedimentary cover includes, similarly to previously discussed basins, the Upper Mesozoic and Cenozoic (Paleogene-Neogene-Quaternary) strata. The sedimentary thickness and structure in this basin are still poorly studied. Sitnikov and Sleptsova (2020) referred the Primorsk and Tastakh basins as the structures formed due to lithospheric deformations during the Mesozoic subduction. In the deepest parts of these depressions, the relics of the transitional types of the crust have been preserved. The edges of the depressions later evolved as autochthonous structures, both representing geologically different types than the initial deformations.

The Chauna basin, located at the western border of the New Siberian – Chukotka orogen, has appeared in the Early Cretaceous. Gresov and Yatsuk (2020) considered this depression as a part of the larger Ayon basin, located offshore and continuing to the continent. Both, the Chauna and Ayon depressions were formed as grabens that appeared in the Early Paleogene. However, in other studies, the Chauna basin is considered as the larger structure that includes the Ayon basin (Drachev et al., 2011; Shipilov, Lobkovsky, 2019; Sitnikov and Sleptsova, 2020). The basin, overlying the folded Early Mesozoic basement, is filled with the Upper Jurassic and Lower Cretaceous coarse-detrital molasses and volcanic rocks (andesites and rhyolites), 2.2 to 2.5 km thick, according to the marine seismic survey (Gresov and Yatsuk, 2020).

The Penzhin basin is located in the Olyutor-Kamchatka belt of Cenozoic folding. This basin is similar in age and composition of the sedimentary and volcanic rocks to other two basins on the Eastern coast of Kamchatka (Il'Pin and Olyutor). The clastic and volcanic rocks of the Late Cretaceous and Cenozoic age form the section of these basins (Ivanov, 1985; Clarke, 1988). In some earlier studies (e.g. Til'man et al., 1969) only the upper structural section is considered. The basement of the Penzhin basin includes the Paleozoic and Mesozoic rocks formed before the pre-Aptian Cretaceous time. The sedimentary fill is of the Late Cretaceous to Cenozoic age.

The Pustorets basin is another depression on the west coast of northern Kamchatka, extending offshore. It is 450 km long and 50–100 km wide, locating on the northwest margin of the Olyutor-Kamchatka, which bounds the Anadyr-Koryak fold system. The folded basement of this basin consists of the Cretaceous rocks (corresponding to nearly all stages of the

Cretaceous period) with the deepest part related to the Aptian-Albian time metamorphosed to greenschist facies and intruded by granite and gabbro in the southeast border. The sediments filling the basin are of the Cenozoic age. The top part of the Cenozoic section is represented by the Oligocene-Miocene sediments; most of them are sandstones and conglomerates. Their thickness is up to 2500 m. The Pustorets basin is bounded on the northwest by the Penzhin-Parapol deep fault and on the southeast by the Vyven deep fault. Within the basin, there exist several highs and lows, which follow the trend of the basin. In the southwest along the shore of the Penzhin Gulf, the Kinkil high, which is 240 km long and about 40 km wide, is located. One can identify three structural sections in this high. The lower one consists of the Paleocene-Eocene sedimentary rocks, the second one is comprised of the Eocene-Oligocene volcanic rocks, and the third section is locally distributed Neogene sediments.

The Anadyr Basin is located at the easternmost part of the study area. It was formed during the Late Mesozoic and Early Cenozoic during the collision of the South Anyui Ocean in the convergence zones of different ages along the Asia continental margin and the Pacific Ocean plate. The folded basement of the basin was formed during the Late Cretaceous (Albian-Cenomanian) orogeny. The evolution history of the sedimentary cover can be divided into three periods: 1) sediments accumulation during the passive continental margin phase (Late Cretaceous – Early Eocene); 2) sediments accumulation in Middle Eocene – Oligocene during the extension and rift formation in the northern part of the basin and compression in its southern part due to the northward movement of the foredeep before the Koryak accretion orogeny; 3) Miocene sediments accumulation in the conditions of continental rifting (Antipov et al., 2008).

The position of the main sedimentary basins in the study area is shown in Fig. 1. This scheme is chiefly based on (Clarke, 1988; Drachev et al., 2016; Drachev, 2011) and on some other publications mentioned above. More details on the structure of the analysed basins will be presented in the Discussion section with the obtained results.

3 Method

As it was mentioned above, in the first stage we compute the isostatic gravity anomalies. By applying this correction, it is possible to remove the effect of deep density anomalies compensating the near surface load (chiefly topography) (e.g. Simpson et al., 1986). This correction is especially useful when we have only a little knowledge about deep structures of the lithosphere. In this case, it is just assumed that the near surface load is compensated according to a plausible isostatic compensation scheme. In spectral domain, the isostatic correction is estimated using the following equation (Kaban et al., 2016, 2017) :

$$\Delta g_{ic}(k_x, k_y) = G_{is}(k_x, k_y) \cdot t_{adj}(k_x, k_y) = -2\pi G\rho \cdot C \cdot \exp(-k \cdot M) \cdot t_{adj}(k_x, k_y), \quad (1)$$

where $k = \sqrt{k_x^2 + k_y^2}$ is the wavenumber, $k_x = 2\pi/\lambda_x$ and $k_y = 2\pi/\lambda_y$, M is the depth to the Moho, G is the gravitational constant. $G_{is}(k_x, k_y)$ is the Green's function (its introduction is explained below). t_{adj} is the adjusted topography, which is introduced to equalize the bathymetry (t_b) and topography variations as well as the initial density variations of sediments for the constant density of the topography ρ:

$$t_{adj} = t_b - \frac{\rho_w}{\rho} t_b - \frac{\rho - \rho_s}{\rho} t_s, \quad (2)$$

where t_s and ρ_s are the thickness and vertically averaged density of sediments from the initial model, ρ_w= 1.03 g/cm³ is the water density. In the continental area, the second term in Eq. (2) is omitted.

It has been demonstrated that the main parameter, which control the style of isostatic compensation, are the average compensation depth (usually associated with the depth to the Moho) and elastic support of the surface load by the lithosphere. The parameter *C* determines the amount of the elastic support (*C*=1 for the local compensation) and depends on the EET (T_e) and wavenumber (Turcotte and Schubert, 1982):

$$C = \Delta\rho g/(k^4 D + \Delta\rho g), \quad (3)$$

where $D = ET_e^3/[12(1-v^2)]$ is the flexural rigidity, v is the Poisson ratio, E is the Young modulus, $\Delta\rho$ is the average density difference between topography and the upper mantle, and g is the gravitational acceleration.

We use a Green's function method (Wienecke et al., 2007; Braitenberg et al., 2002; Dill et al., 2015) instead of a direct application of Eq. (1) in the spectral domain, since the direct application is impossible in the case of variable depth to the Moho and EET. The above authors demonstrated that this approach is appropriate in this case. The isostatic correction is estimated in a sliding window as a convolution of the adjusted topography with the Green's functions $G_{is}(x, y, M, T_e)$ for corresponding $M(x_0,y_0)$ and EET ($T_e(x_0,y_0)$). Then, the isostatic anomalies are calculated as follows:

$$\Delta g_i(x_0, y_0) = \Delta g_b(x_0, y_0) + \iint_{-1250km}^{1250km} t_{adj}\,(x_0 + x, y_0 + y) \cdot G_{is}(x, y, M(x_0, y_0), T_e(x_0, y_0))dxdy, \quad (4)$$

where $\Delta g_b(x, y)$ is the Bouguer gravity anomaly. The radius of the sliding window is extended to 1250 km to avoid boundary effects (Kaban et al., 2021a,b).

In the second stage, the decompensative correction (Δg_{dc}) is calculated following (Kaban et al., 2017):

$$\Delta g_{dc}(k_x, k_y) = \frac{1}{\exp(k \cdot M)/C - 1} \Delta g_i(k_x, k_y), \quad (5)$$

where Δg_i are the isostatic anomalies. By applying this correction, it is possible to reduce the effect of compensation of the unknown density anomalies in the upper crust, which are still missed in the initial model. Otherwise the total effect of the upper crust anomalies and their compensation tends to zero already for the basins with a horizontal size of several hundred kilometres or more (e.g. Kaban et al.. 2021a).

Unfortunately, the decompensative correction increases to infinity with increasing of the wavelength. Following Cordell et al. (1991) we reduce it after a predefined wavelength (λ_0=1500 km) (Kaban et al., 2017, 2021a). This restriction doesn't bias the result because it is assumed that wide basins are already included in the initial model. Like for the isostatic anomalies, we apply the Green's function method to estimate the decompensative correction. A sum of the isostatic anomalies and this correction gives the decompensative gravity anomalies.

4. Computation of the isostatic and decompensative gravity anomalies

4.1 Initial data

As the initial data, in this study we use the Bouguer gravity anomalies, topography, initial model of sediments (thickness and vertically averaged density), EET of the lithosphere, and depth to the Moho. For calculations, all the data have been converted to the orthographic projection with the resolution 10x10 km.

The observed gravity field (Fig. 2a) is based on the EIGEN-6c4 model (Förste et al., 2014) that represents a combination of the recent satellite missions and surface/airborne observations. The maximal resolution is 2190 spherical harmonics degree/order (≈5′ x 5′ in space); however the actual resolution depends on available surface observations. It is important that up to a resolution of approximately 70 km this field is based on the satellite data only (Förste et al., 2014), which guarantees complete and homogeneous coverage sufficient for the present study. The topography/bathymetry is represented by the downscaled ETOPO-1 model (Amante & Eakins, 2008). For computation of the Bouguer anomalies, the topography density is assumed 2.67 g/cm^3, and for the water – 1.03 g/cm^3 (–1.64 g/cm^3 relative to the standard density of the uppermost layer). The gravity effect of the topography/bathymetry has been calculated within the radius 333.6 km (3 degrees) based on the initial topography/bathymetry grids. The increase of this radius would produce only long-wavelength anomalies, which are not considered in the manuscript as described above.

The initial thickness of sediments is presented in Fig. 2b. For the oceans, we employed a recent high-resolution global compilation of Straume et al. (2019). For the initial densities, we used a density-depth relation for typical offshore basins from Mooney and Kaban (2010). For the continents, the data of Stolk et al. (2013) have been implemented west of 150° E, and for the eastern part from (Kaban, 2001). These papers also provide vertically averaged densities for each point of the grid. The gravity effect of the initial model of sediments is additionally separated from the Bouguer anomalies. The final residual anomalies are shown in Fig. 3a.

Based on these data, we have also estimated the adjusted topography (Eq. (2), Fig. 3b), which finally represents a unified surface load with the standard density of topography (2.67 g/cm^3). In particular, vast continental areas are characterized by negative adjusted topography due to the presence of low-density sediments.

For the continental part, the Moho boundary (Fig. 4a) is based on the same data sources as the initial model of sediments (Stolk et al., 2013; Kaban, 2001). For the Arctic Ocean, the Crust1.0 model is employed (Laske and Masters, 2013). It has been demonstrated that plausible changes of the Moho model don't affect the result significantly (Kaban et al., 2021a).

The effective elastic thickness of the lithosphere (Fig. 4b) is taken for the continental part and shelf from (Tesauro et al., 2012). Contrary to the Moho, this parameter might significantly influence the final estimations (Kaban et al., 2021a). Tesauro et al. (2012) have globally compared EET obtained with independent methods (geomechanical modeling and cross-spectral analysis of the gravity field and topography). For the study area, both methods produce very similar results, which proves that EET determinations are sufficiently robust. Here we employ the map based on the geomechanical modelling. For

the rest of the Arctic Ocean a simple relationship with the lithosphere age ($T_e = 2.7\sqrt{age}$) is employed (Calmant et al., 1990). The age data are taken from (Müller et al., 2008).

4.2 Results

The data described in the previous section have been used to compute the isostatic correction (Fig. 5a). It is dominated by long- and mid-wavelengths since the effect of small-scale compensation is reduced due to the large EET of the lithosphere and deep Moho. By adding the isostatic correction to the Bouguer anomalies (with the removed effect of the initial model of sediments) we obtain the isostatic gravity anomalies. At the long-wavelengths, these anomalies still contain dynamic effects induced by mantle convection or glacial-isostatic adjustment (Kaban et al., 1999, 2004). It was earlier demonstrated that this component could be reduced by applying a Gauss-type filter with a boundary wavelength (half amplitude) of about 1500-2500 km. As it was mentioned before, we do not consider such extended anomalies, therefore this filtering would not affect final corrections for the initial sedimentary model. The residual isostatic anomalies corrected for the effect of the initial model of sediments are displayed in Fig. 5b.

As it is visible from Fig. 5b, only small-scale anomalies (or narrow) are typically presented in this field. As was suggested above, this is due to partial isostatic compensation of the upper crust density anomalies. In the next stage, we apply the decompensative correction to reproduce a full effect of the near-surface density variations.

The final decompensative correction and decompensative gravity anomalies are shown in Fig. 6a and 6b, respectively.

5 New models of the sedimentary thickness and density

Based on the computed decompensative gravity anomalies we have corrected the initial model of the sedimentary cover. In this study we construct two models. In the first one, it is assumed that the whole gravity effect shall be explained by changes of the sedimentary thickness. In the second model, we use the same approach as in (Kaban et al., 2021b) and equally attribute the decompensative anomalies to changes of the thickness and average density of sediments.

In addition, several limitations have been forced to keep the model realistic (Kaban et al., 2021b):

1. It is assumed that sedimentary thickness should not exceed 20 km, the limit, which is suggested based on existing seismic studies.
2. The maximal reduction of the sedimentary thickness is limited to 0.75 of the initial one.
3. For the second model, the final density of sediments (averaged with depth) should be within the range 1.9-2.72 g/cm^3, which is consistent with experimental data (e.g. Kaban and Mooney, 2001).

Due to the above constraints, it was not always possible to explain the whole decompensative anomaly by changes of the initial model of sediments. In this case, the remaining part was attributed to the uppermost layer of the crystalline crust. For determination of necessary corrections, we used a typical density depth curve based on compaction relationships (Mooney and Kaban, 2010). This procedure is explained in Fig. 7. The first point at the curve represents the sedimentary thickness

according to the initial model. Then, we determined the corrected thickness, which fits the decompensative anomaly according to this density-thickness relationship (Fig. 6b). Therefore, the correction is non-linear and increases with the increase of the initial depth. In case of the second model, the required density correction was simply determined by dividing half of the decompensative anomaly by the corrected thickness (limited if necessary) with the coefficient $2\pi G$.

In the first adjusted model (Fig. 8a), several significant changes are visible, comparing to the initial thickness of sediments (Fig. 2b). The second model (Fig. 8b) also displays some changes comparing to the initial sedimentary thickness. The new model shows not only redistribution of the sedimentary thickness, but some changes that, as we suppose, refer to structure of crystalline crust, since we cannot completely divide these effects in the decompensative anomalies. Some of the new details on the sedimentary thickness distribution generally match the surface geology: however, some issues may raise questions, which are discussed in the next section.

6 Discussion

6.1 Sedimentary cover: model 1

The obtained models of the sedimentary cover generally repeat the large-scale features of the sedimentary thickness; however, some essential changes are visible. To display these details, we have prepared a set of the maps zooming up some important regions. In Fig. 9, we provide a comparison between the initial sedimentary model (in the left) and two new models (the first model in thecenter and the second one in the right).

In the model 1 (Fig. 8a), several areas of relatively large thickness (3–4 km) are found in the Chukotka mountain area. They are likely related to thick volcanogenic deposits of relatively low density formed during the OCVB development. This zone continues as a 1–2 km deep conduit, bounding the continental Chauna basin from the south. Then, this zone, with a characteristic thickness of 0.5–2 km, continues southwest and reaches the Okhotsk Sea, repeating the OCVB shape and bounding its structures (e.g., the eastern slope of the Kolyma Mountains).

The thickness of many sedimentary basins has been significantly reduced in the new model compared to the initial one. Also, for some basins, the location of depocenters has been changed. For example, the sedimentary thickness has been reduced in the Anadyr basin (Fig. 9a, center), especially in its continental part (to 1–2 km). Moreover, the deepest part of the continental Anadyr basin is shifted southeast in the new model, still remaining within the continent, while the deepest part (the depocenter) of the eastern segment, located within the sea shelf, remains in the same place as in the initial model. We refer the corresponding gravity effect of the sedimentary cover mainly to the Cenozoic sediments, less consolidated than the deeper Mesozoic strata. Antipov et al. (2008) demonstrate a regional map of the sedimentary thickness for the Anadyr basin, which is also different from the initial one shown in Fig. 2b. Their model is based on several short (several tens of km) common depth point (CDP) seismic profiles, no other seismic data are available for this structure. These profiles show high variability of the basement from 0.5-1 km to 4 km at some local points, although the interpretation of reflectors is somewhat uncertain. The thickness of sediments is also reduced in the northern part of the basin like in our model. Although the

thickness is higher in some very local depressions (Antipov et al., 2008), which are not resolved by the new model, the northward decrease trend is visible for the continental part in both models, indicating that the new modelling approach provides sufficiently reliable results, at least qualitatively.

In the new model, the thickness of the Penzhin basin (Fig. 9b, center) has been also reduced in the central part by about two times, however, it remains nearly the same near the borders. In contrast, the Pustorets basin thickness is increased up to about 4 km compared to 2-3 km according to Clarke (1988), and the basin depocenter is shifted to the southeast in the new model, being a part of the relatively deep zone continuing to the eastern coast of the Kamchatka Peninsula. However, the study of Clarke (1988) is an unpublished review not providing specific information about the data sources and especially of the methods.

Next, the new model displays a slight increase in thickness in the northern continental part of the Chauna basin (Fig. 9c, center) comparing to the initial model (Fig. 9c, left). In the continental margin of the basin, the Cenozoic sedimentary thickness matches the drilling results (approximately 670 m including about 490 m of the Paleogene sediments, Aleksandrova (2016)). The sedimentary thickness in the offshore part of the basin referred as the Ayon basin (Fig. 9c) has been reduced to 2-2.5 km comparing to the initial model, in which it reaches 4 km. Note that the new model agrees with the results of the seismic survey for the Ayon basin, as seen in the map of Gresov and Yatsuk (2020), in which the Ayon thickness is also about 2.2–2.5 km. For the rest of the basin, the thickness distribution is nearly the same and increases from southeast to northwest.

We have found the most significant changes for the Zyryanka basin (Fig. 9d). In the new model (Fig. 9d, center), the basin is divided into three separate segments of approximately 2-2.5 km sedimentary thickness. Two of these separate segments correspond to the largest coal-bearing zones within the Zyryanka depression according to the map of Koporulin (1979) — the Myatis zone (northwestern one) and the Zyryanka-Silyapsk zone (southeastern one). Obviously, these zones, contoured with dashed lines on Fig. 9d, outline the Lower Cretaceous sedimentation. Like in the initial model, the southeastern part of the Zyryanka basin is deeper than the northwestern one. Remarkable changes of the thickness have been found in the northwestern segment. According to the new model, the 2–3 km thick northwestern segment of the basin (the Myatis zone), is geometrically different from that one given in (Koporulin 1979). It is divided into two branches at an almost right angle with respect to the main direction of this structure, and the newly revealed branch of slightly lower thickness is pointing northeast. As seen on the map from (Koporulin, 1979), another small zone of distribution of the Lower Cretaceous coal-bearing deposits, unidentified in the initial model, is located northeast from the Myatis zone (Fig. 9d), which supports again the new model. The last one shows a connection of these zones, although the shape of this northeastern branch is not so clearly traced as compared to the segment related to the Zyryanka-Silyapsk zone. Although the map of Koporulin (1979) generally matches the shape of the new founded sedimentary thickness distribution, it was based on relatively old and geological studies and drilling data. It was mentioned by the author that the geological mapping and lithological-facies analysis of the basin strata, including the coal-bearing zones, was done by him and his predecessors in 1960-1970's with significantly different detail; therefore, some areas of the basin have been insufficiently studied. This gives a reason to

conclude that the lateral sedimentary thickness redistribution in the Zyryanka basin is a new finding, showing the features of the Lower Cretaceous strata that were not previously mapped due to their overlap with the Cenozoic sediments and relatively sparse data.

It should be noted that previous studies demonstrate significant differences and contradictions in mapping the sedimentary thickness for the Zyryanka basin. Sitnikov et al. (2017) argues that the Lower Cretaceous sediments are up to 8 km thick in several parts of this depression, and that the Cenozoic sediments are more than 3 km thick. Similar conclusions for the maximal sedimentary thickness of 7–9 km were made earlier by Koporulin (1979). Stoupakova et al. (2017) mention even 8–10 km of the total thickness. However, neither the initial sedimentary model used in this study nor the sedimentary map for the Arctic (Petrov et al., 2016) indicate such thickness of sediments in the Zyryanka basin. Actually, most of the old maps are based on very sparse, unsystematic and obsolete results based on outdated methods, e.g. interpretation of the Bouguer gravity anomalies or magnetic data. Our study shows that the sedimentary thickness should be about 3 km lower in the deepest parts.

The Primorsk basin (Fig. 9e) is also poorly studied by seismic surveys (Pavlova, 2020), which revealed only the basic features of the sedimentary structure for shallow depths often not reaching the basement. According to these seismic data, the uppermost layers are represented by Neogene-Quaternary sediments (including alluvial) up to 1.2 km thick and the underlying Meso-Cenozoic sediments up to 2 km thick. It is clear that the new model (Fig. 9e, center) generally agrees both with the initial one (Fig. 2b) and with the results obtained from the sparse seismic studies, and the sedimentary thickness of the Primorsk basin remains almost the same as in the initial model for its deepest part (2–2.2 km). However, the thickness of the Primorsk basin is significantly reduced in its southeastern part. This lateral variability the sedimentary thickness is discovered for the first time in the present study.

The maximal sedimentary thickness of the Tastakh basin (Fig. 9e) is about 2.5–3 km in its depocenter according to the new model. From the comparison of the initial model (Fig. 9e, left) and the new one (Fig.9e, center), no significant changes in the sedimentary thickness appeared after the decompensation correction, and the basin shape remains the same. Sitnikov (2017) and Sitnikov and Sleptsova (2020) also ipointed the sedimentary thickness values from 1.5 to 3 km for the basin. The Lower Jurassic rocks at the bottom of the CDP transect presented in (Sitnikov, 2017) can be considered as a relatively dense transition layer between the basement and the sedimentary cover, which gives only a little effect in the gravity field; and this is the reason why the new sedimentary model does not show depths of more than 3 km for this basin. The segment of the Laptev-Moma system in the studied area, including the rifts filled with Cenozoic sediments, was not changed significantly.

Potential uncertainties of the obtained model increase with depth since the difference in density with the crystalline rocks is insignificant for deep layers and even relatively thick sediments produce only a small effect in this case. Therefore, even an insignificant negative decompensative anomaly could lead to a noticeable increase of the basement's depth, if it was initially deep (Fig. 7). For example, the density of Late Cretaceous sediments in the region might be quite large, especially in the intermontane depressions, due to the Late Mesozoic and even Cenozoic metamorphism. In the Eastern part, the basins bounding the OCVB could include the Cretaceous layer as a transition between the folded basement and less dense upper

layers. This factor could also lead to significant differences with seismic models, which interpret relatively high seismic wave velocities in the lower (ancient) part of the sedimentary cover as the basement (e.g. for shallow Lower Cretaceous deposits in the Verkhoyansk region). So, for the deep basins, the model should be considered rather qualitative than quantitate. Finally, an additional gravity effect can be associated not only with sedimentary layers but also with the upper part of the crystalline crust, resulting in artificial increase of the sedimentary thickness in the final model.

Potential uncertainties of the sedimentary thickness determined from the decompensative gravity anomalies were assessed by Kaban et al. (2021a). They assume that the uncertainty of the density-depth relation is approximately 15% (Mooney and Kaban, 2010). Then, for the thickness 2 km, actual values would be in the interval 1.55-2.6 km; and for the thickness 4 km – within 2.9-5.35 km. For deep basins (approximately > 7.5 km), the upper limit is indefinite. Therefore, for the depths larger than 7 km, the thickness estimations are rather qualitative.

6.2 Sedimentary cover: model 2

In the second model (Fig. 8b), we assumed that half of the decompensative anomaly is related to the changes of the sedimentary thickness, and the other half to the density of sediments. Despite some changes in the thickness, qualitatively, its distribution remained similar to the first model.

In the second model, the OCVB zone is within 1.2–2 km and traced at the same position as in the first model. However, due to the different initial conditions, this zone is smoother and has fewer small-scale details, although they generally repeat the OCVB shape. The main depressions zone is now wider. Like in the first model, the thickness of sediments is reduced in the Zyryanka basin and, in general, in the Primorsk and Tastakh basins, but, at the same time, their outlines remain almost the same as in the first model. The thickness of the offshore part of the Chauna basin (its Ayon segment) has been decreased by 2 times compared to the initial model (Fig. 9c).

Some significant differences in thickness and shape are found for the Anadyr basin (Fig. 9a, right). The maximal thickness in the second model is shifted to the southeast less than in the first model, but in both cases its position differs from that one in the initial model. At the same time, the position of the depocenter of the offshore part is basically the same in all three models. Possible reasons for the migration of the continental thickness maximum of the Anadyr basin in both corrected models might be related to the heterogeneous structure of its folded basement and of the deep sedimentary layers (Clarke, 1988). The northern and northwestern parts of the basement mainly consist of the Late Cretaceous OCVB rocks (effusives, tuffs, etc.), while its southeastern part formed in the in the conditions of the Okhotsk-Chukotka active continental margin from the end of the Early Cretaceous to the beginning of the Late Cretaceous, when the adjacent Koryak (Anadyr-Koryak) folded system formed as an accretionary prism of the subduction zone. The lower layers of the sedimentary cover are presented in the south and southwest, close to the Koryak folded system, and are of the Albian-Cenomanian, later Upper Cretaceous and Early Paleocene age. These strata are often considered as a transition layer between the basement and sediments (Antipov et al., 2008). Moreover, the Cenozoic section, contributing to the main 2–3 km part of the cover, is distributed wider than the above mentioned transition complex with thickness decreasing from south to north. Application of

the decompensative corrections reveals these lateral sedimentation irregularities and leads to the changes of the thickness in both resulting models.

The thickness variations in the Pustorets basin in the second model (Fig. 9b, right) are close to the initial model (Fig. 9b, left), while the absolute thickness is generally lower than in the first model, with smoother variations. The depocenter position is similar to the first model (Fig. 9b, left). The Penzhin basin location was not changed, although the sedimentary thickness is reduced (Fig. 9b, right). Finally, the sedimentary structure of the Laptev-Moma system (Shiroston and Ust'-Yana rifts) in the second model remains nearly the same as in the first model. The reason for this is the relatively insignificant depth of the sedimentary strata filling the rifts: it is about 1–2 km, as mentioned in (Drachev et al., 2010; Drachev, 2016), and it is reduced to 1 km or even less on the basement height between the Shiroston and Ust'-Yana grabens. The density of the sediments filling the rift is relatively high.

The corrections for the initial density of sediments (Fig. 10a) are within the range of –0.7 to 0.9 g/cm^3. The obtained sedimentary density model (Fig. 10b), in our opinion, should be interpreted rather qualitatively, than quantitatively, as the density of sediments is vertically averaged and potentially anomalous layers are not identified. The calculated density distribution generally matches the new features of the sedimentary thickness after the decompensative correction. For example, the 2.2–2.4 g/cm^3 zone corresponding to the Zyryanka basin (Fig. 11) repeats the shape of the new thickness map based on the decompensative gravity anomalies. The results show a clear relation between the northwestern zone of the Lower Cretaceous coal-bearing molasses and the larger Myatis zone (the corresponding zones are contoured by dashed lines in Fig. 11). It is visible in the map (Fig. 10b) that the average density of sediments increases with thickness due to compaction under the increased pressure. Large density changes are also related to the mountain areas of the Verkhoyansk orogeny (e.g. the Chersky Ridge) and the OCVB structures in its northern segment. The difference between the density of these structures and the density of thick sediments is moderate.

The new sedimentary models were calculated based on the assumption that the decompensative anomalies are exclusively induced by changes in the sedimentary basins' structure (thickness in the first model and both, thickness and density, in the second one) by applying the approach of Kaban et al. (2021b). Another possible source of the decompensative anomalies, especially in the case of positive ones, could be local densification of the upper crust due to intrusive rocks or metamorphism, which effects were not considered in this study. Therefore, the resulting models may include possible local uncertainties in the vicinity of the intrusions related to the OCVB structure. However, for most of the sedimentary basins in the study area, these uncertainties are generally local and, therefore, minor with respect to the large-scale structures.

Conclusions

This study presents the new sedimentary cover models for the Eastern Asia Arctic zone based on the analysis of the decompensative gravity anomalies. First, we computed the isostatic gravity anomalies for the study area, and then we applied the decompensative correction to the isostatic anomalies. The correction spans within a range of –50 to +30 mGal and

principally changes the isostatic anomaly patterns. Two sedimentary cover models, differing in their initial conditions, have been obtained from the decompensative anomalies. The main discoveries are as follows:

1. Essential changes in the sedimentary thickness and the depocenter location have been found for the Anadyr basin in its continental part, where the thickness has been reduced to 1–2 km.
2. New details of the sedimentary thickness variations have been revealed for the central part of the Penzhin basin, where the thickness appeared to be lower by about two times comparing to the initial model, and for the Pustorets basin, for which the new location of the depocenter has been identified.
3. For the offshore part of the Chauna basin (referred as the Ayon basin), the sedimentary thickness has appeared to be 2-2.5 km in the new model, which is lower than in the initial model (4 km). The new result agrees with the marine seismic surveys, which confirms robustness of the method.
4. The most significant lateral redistribution of the sedimentary thickness has been found for Lower Cretaceous coal-bearing strata in the northern part of the Zyryanka basin. The new model indicates the connection of two coal-bearing zones, revealing the features of the Lower Cretaceous strata that were not previously mapped due to insufficient geological surveys.
5. New details on the sedimentary thickness variations have been discovered for the Primorsk basin. The sedimentary thickness in the basin is significantly reduced in the southeast direction.

As we mentioned before, it is impossible to completely separate the effects of the sedimentary cover density anomalies from those ones in the upper crust. Therefore, the new models may display some artificial features, which appear due to neglecting the crystalline crust density heterogeneity. Nevertheless, the overall analysis of two new models confirms the efficiency of the approach based on the decompensative gravity anomalies. This approach application has made it possible to reveal several essential changes in the geological structure of the analysed sedimentary basins. In many cases, the results of our study are the only ones providing the information on the structure of sedimentary basins.

In the interpretation of the obtained models, some issues remain unexplained. For example, the rocks of similar age forming the basins are sometimes considered here in different ways, because the tectonic development of the study area was different and its relatively younger segments were formed in its Eastern part. For the Anadyr, Penzhin, and Pustorets basins, the Cretaceous rocks form the folded basement, while most of the Eastern part of the study area is covered by the volcanic rocks (of the late Early Cretaceous – Late Cretaceous age and younger), resulting in reduced sedimentary cover in both new models.

Previous geophysical studies in the region under consideration are very sparse and represented by old and unsystematic results. Furthermore, the employed indirect geophysical methods (gravity, magnetic) are outdated, while direct seismic data are available only for limited locations. Thus, despite detailed surface geology surveys, the sedimentary thickness is still poorly mapped in the whole region. The present study provides for the first time a consistent map for the whole Arctic zone of northeastern Asia based on unified standards of interpretation. It confirms that this method can be used for investigations of hardly accessible areas as it was previously done for Antarctica (Haeger and Kaban, 2019) and for the Congo basin

(Kaban et al., 2021a). Finally, the obtained results can be used for the future planning of detailed studies of local structures within the study region, which have potential for mineral prospecting and exploitation and for the infrastructure development important for the Arctic zone.

Data availability

All the datasets presented here are based on the initial data from public domain resources. The obtained results, including the Bouguer gravity anomalies, residual gravity field, adjusted topography, isostatic and decompensative corrections and anomalies used for their calculation, new sedimentary thickness and density models. are available at the World Data Center for Solar-Terrestrial Physics website http://www.wdcb.ru/arctic_antarctic/arctic_grav_1.html.

Author contributions

Conceptualization performed by Mikhail K. Kaban, Alexei D. Gvishiani, Anatoly A. Soloviev, Roman V. Sidorov and Alexei G. Petrunin. Modelling methodology developed by Mikhail K. Kaban. Investigation and formal analysis done by Roman V. Sidorov and Mikhail K. Kaban. Alexei D. Gvishiani, Anatoly A. Soloviev and Roman I. Krasnoperov organized the funding acquisition and resources. Data curation work done by Mikhail K. Kaban, Anatoly A. Soloviev, Roman I. Krasnoperov, Anton B. Popov and Alexei G. Petrunin. Visualization provided by Anton B. Popov. Original draft prepared by Roman V. Sidorov, Mikhail K. Kaban and Alexei A. Oshchenko. All the authors were involved in the review and editing of the manuscript text.

Competing interests

The authors declare that they have no conflict of interest.

Acknowledgements

This work employed data and services provided by the Shared Research Facility “Analytical Geomagnetic Data Center” of the Geophysical Center RAS (http://ckp.gcras.ru/). The research was funded by the Russian Science Foundation (project No. 21-77-30010).

References

Aleksandrova, G. N.: Geological evolution of Chauna Depression (North-Eastern Russia) during Paleogene and Neogene. 1. Paleogene, Bulletin of Moscow Society of Naturalists. Geological Series, 91, 148-164 (in Russian), 2016.

Amante, C., Eakins, B. W.: ETOPO1 1 Arc-Minute Global Relief Model: Procedures, Data Sources and Analysis. National Geophysical Data Center, NESDIS, NOAA, U.S. Department of Commerce: Boulder, CO, USA, 2009. Access online: https://www.ngdc.noaa.gov/mgg/global/relief/ETOPO1/docs/ETOPO1.pdf (accessed on 12.10.2020).

Andieva, T. A.: Tectonic position and main structures of the Laptev Sea, Neftegazovaya Geologiya. Theory and practice, 3, (in Russian) URL: http://ngtp.ru/rub/4/8_2008.pdf (accessed on 12.05.2020), 2008.

Antipov, M. P., Bondarenko, G. E., Bordovskaya, T. O., and Shipilov, E. V.: Anadyr basin (the north-east of Eurasia, the Bering Sea coast): geological structure, tectonic evolution and oil-and-gas bearing: Apatity: Publ. Kola Science Centre RAS, 53 p. (in Russian), 2008.

Blakely, R. J.: Potential Theory in Gravity and Magnetic Applications. Cambridge University Press Science - 4: London, Great Britain, 1995.

Braitenberg, C.; Ebbing, J.; Götze, H. J.: Inverse modelling of elastic thickness by convolution method - The eastern Alps as a case example, Earth Planet. Sc. Lett., 202, 387–404. https://doi.org/10.1016/S0012-821X(02)00793-8, 2002.

Calmant, S., Francheteau, J., & Cazenave, A.: Elastic layer thickening with age of the oceanic lithosphere: a tool for prediction of the age of volcanoes or oceanic crust, Geophys. J. Int., 100, 59-67, https://doi.org/10.1111/j.1365-246X.1990.tb04567.x, 1990.

Clarke J. W.: Sedimentary basins of Northeastern USSR, US Department of the Interior, Geological Survey, URL: https://pubs.usgs.gov/of/1988/0264/report.pdf (accessed on 18.04.2021), 1988.

Cordell, L.; Zorin, Y. A.; Keller, G. R.: The decompensative gravity anomaly and deep structure of the region of the Rio Grande rift, J. Geophys. Res.: Solid Earth (1978–2012), 96, 6557-6568, https://doi.org/10.1029/91JB00008, 1991.

Dill, R.; Klemann, V.; Martinec, Z.; Tesauro, M.: Applying local Green's functions to study the influence of the crustal structure on hydrological loading displacements, J. Geodyn., 88, 14-22. https://doi.org/10.1016/j.jog.2015.04.005, 2015.

Drachev, S. S.: Fold belts and sedimentary basins of the Eurasian Arctic, Arktos, 2, 21, https://doi.org/10.1007/s41063-015-0014-8, 2016.

Drachev, S. S.:Tectonic setting, structure and petroleum geology of the Siberian Arctic offshore sedimentary basins, in: Geological Society London Memoirs, 35(1): 369-394, https://doi.org/ 10.1144/M35.25, 2011.Drachev, S. S., Malyshev, N. A., Nikishin, A. M.: Tectonic history and petroleum geology of the Russian Arctic Shelves: an overview, Petroleum Geology Conference series, 7, 591-619, https://doi.org/10.1144/0070591, 2010.

Ebbing, J., Braitenberg, C., Wienecke, S.: Insights into the lithospheric structure and the tectonic setting of the Barents Sea region from isostatic considerations, Geophys. J. Int. 171, 1390-1403, https://doi.org/10.1111/j.1365-246X.2007.03602.x, 2007.

Förste, C., Bruinsma, S. L., Abrikosov, O., Lemoine, J.-M., Marty, J. C., Flechtner, F., Balmino, G., Barthelmes, F., Biancale, R.: EIGEN-6C4 The latest combined global gravity field model including GOCE data up to degree and order 2190 of GFZ Potsdam and GRGS Toulouse, GFZ Data Services :Potsdam, Germany, https://doi.org/10.5880/icgem.2015.1, 2014.

Grachev, A. F., Demenitskaya, R. M., Karasik, A. M.: The Middle Arctic Ridge and its continuation to the continent, Geomorfologiya, 1, 42-45 (in Russian), https://doi.org/10.15356/0435-4281-1970-1-42-45, 1970.

Gresov, A. I., Yatsuk, A. V.: Geochemistry and genesis of hydrocarbon gases of the Chaun depression and Ayon sedimentary basin of the East Siberian Sea, Russian Journal of Pacific Geology, 14, 87-96, https://doi.org/10.1134/S1819714020010042, 2020.

Haeger, C., Kaban, M. K.: Decompensative Gravity Anomalies Reveal the Structure of the Upper Crust of Antarctica, Pure Appl. Geophys., 176, 4401–4414, https://doi.org/10.1007/s00024-019-02212-5, 2019.

Hildenbrand, T. G., Griscom, A., Van Schmus, W. R., Stuart, W. D.: Quantitative investigations of the Missouri gravity low: A possible expression of a large, Late Precambrian batholith intersecting the New Madrid seismic zone, J. Geoph. Res., 101(B10), 21921–21942, https://doi.org/10.1029/96JB01908, 1996.

Ivanov, V. V.: Sedimentary Basins of Northeastern Asia, Trofimuk, AA, Ed. (in Russian), 1985.

Jachens, R. C., Moring, C.: Maps of the thickness of Cenozoic deposits and the isostatic residual gravity over basement for Nevada, U.S. Geological Survey Open File Report, 90-404, https://doi.org/10.3133/ofr90404, 1990.

Kaban, M.: A Gravity Model of the North Eurasia Crust and Upper Mantle: 1. Mantle and Isostatic Residual Gravity Anomalies, Russian Journal of Earth Sciences, 3, https://doi.org/10.2205/2001ES000062, 125-144, 2001.

Kaban, M. K., Delvaux, D., Maddaloni, F., Tesauro, M., Braitenberg, C., Petrunin, A. G., and El Khrepy, S.: Thickness of sediments in the Congo basin based on the analysis of decompensative gravity anomalies. Journal of African Earth Sciences, 104201, 179, https://doi.org/10.1016/j.jafrearsci.2021.104201, 2021a.

Kaban, M. K., Gvishiani, A., Sidorov, R., Oshchenko, A., Krasnoperov, R. I.: Structure and Density of Sedimentary Basins in the Southern Part of the East-European Platform and Surrounding Area, Appl. Sci., 11, 512, https://doi.org/10.3390/app11020512, 2021b.

Kaban, M. K., El Khrepy, S., Al-Arifi, N.: Importance of the Decompensative Correction of the Gravity Field for Study of the Upper Crust: Application to the Arabian Plate and Surroundings, Pure Appl. Geophys., 174, 349-358. https://doi.org/10.1007/s00024-016-1382-0, 2017.

Kaban, M. K., El Khrepy, S., Al-Arifi, N.: Isostatic Model and Isostatic Gravity Anomalies of the Arabian Plate and Surroundings, Pure Appl. Geophys., 173, 1211–1221, https://doi.org/10.1007/s00024-015-1164-0, 2016.

Kaban, M.K.; Mooney, W.D.: Density structure of the lithosphere in the Southwestern United States and its tectonic significance, J. Geophys. Res., 106, 721–740, https://doi.org/10.1029/2000JB900235, 2001.

Kaban, M. K., Schwintzer, P., Reigber, Ch.: A new isostatic model of the lithosphere and gravity field, J. Geodesy, 78, 368-385, https://doi.org/10.1007/s00190-004-0401-6, 2004.

Kaban, M. K., Schwintzer, P., Tikhotsky, S. A. Global isostatic residual geoid and isostatic gravity anomalies, Geophys. J. Int., 136, 519-536, https://doi.org/10.1046/j.1365-246x.1999.00731.x, 1999.

Koporulin, V. I.: Accumulation conditions and lithogenesis of the Lower Cretaceous deposits of the Zyryanka basin, Geological Institute of the USSR Academy of Sciences: Transactions, Vol. 338, Moscow: Nauka. 181 p. (in Russian), 1979.

Langenheim, V. E., Jachens, R. C.: Gravity data collected along the Los Angeles regional seismic experiment (LARSE) and preliminary model of regional density variations in basement rocks, southern California, U.S. Geological Survey Open File Report, 96-682, https://doi.org/10.3133/ofr96682, 1996.

Laske, G., Masters, G.: Update on CRUST1.0 —A 1-degree global model of Earth's crust, Geophysical Research Abstracts, 15, EGU2013-2658, 2013.

Mooney, W.D., Kaban, M. K.: The North American Upper Mantle: Density, Composition, and Evolution, J. Geophys. Res., 115, B12424. https://doi.org/10.1029/2010JB000866, 2010.

Morozov, O.L.: Geological structure and tectonic evolution of Central Chukotka, Geological Institute of the Russian Academy of Sciences: Transactions, Vol. 523, Moscow: GEOS, 208 p. (in Russian), 2001.

Müller, R. D., Sdrolias, M., Gaina, C., and Roest, W. R.: Age, spreading rates, and spreading asymmetry of the world's ocean crust, Geochem. Geophy. Geosy., 9, https://doi.org/10.1029/2007GC001743, 2008.

Pavlova, K. A., Sitnikov, V. S.: Main aspects of the geological structure of the East Siberian Lowland, International Research Journal: Earth Sciences, 12, 41-44, https://doi.org/10.23670/IRJ.2020.102.12.041, 2020.

Petrov, O., Shokalsky, S., Kashubin, S., Sobolev, N., Petrov, E., Sergeev, S., Morozov, A., Artemieva, I. M., Ernst, R. E., Smelror, M.: Crustal structure and tectonic model of the Arctic region, Earth Sci. Rev., 2016. Vol. 154. P. 29-71.

Shipilov, E. V., Lobkovsky, L. I.: Core elements of tectonics of the Eastern Arctic continental margin of Eurasia, Fersmanov Scientific Session of the GI KSC RAS: Proceedings, 16, 615-619, 2019.

Simpson, R. W., Jachens, R. C., Blakely, R.J., Saltus, R. W.: A new isostatic residual gravity map of the conterminous United States with a discussion on the significance of isostatic residual anomalies, J. Geoph. Res., 91, 8348-8372, https://doi.org/10.1029/JB091iB08p08348, 1986.

Sitnikov, V. S., Alekseev, N. N., Arzhakov, N. A., Obolkin, A. P., Pavlova, K. A., Sevostyanova, R. F., Sleptsova, M. I.: About the structure and prospects for oil and gas bearing of the coastal arctic territories of Eastern Yakutia, Science and education, 4, 50-59 (in Russian), URL: https://cyberleninka.ru/article/n/o-stroenii-i-perspektivah-neftegazonosnosti-prishelfovyh-arkticheskih-territoriy-vostochnoy-yakutii (last visited: 08.05.2021), 2017.

Sitnikov, V. S., Sleptsova M. I.: On the potential oil-and-gas-bearing territories of the North-East of Yakutia, International Research Journal: Geology and Mineralogy, 12, 21-24. https://doi.org/10.23670/IRJ.2020.102.12.037, 2020.

Stolk, W., Kaban, M. K., Beekman, F., Tesauro, M., Mooney, W. D., Cloetingh, S.: High resolution regional crustal models from irregularly distributed data: Application to Asia and adjacent areas, Tectonophysics, 602, 55–68, https://doi.org/10.1016/j.tecto.2013.01.022, 2013.

Stoupakova, A. V., Suslova, A.A., Bolshakova M.A., Sautkin, R.S., Sannikova, I.A.: Basin analysis for the search of large and unique fields in the Arctic region, Georesources, 19-35 (in Russian). http://doi.org/10.18599/grs.19.4, 2017.

Straume, E. O., Gaina, C., Medvedev, S., Hochmuth, K., Gohl, K., Whittaker, J. M., Fattah, R. A., Doornenbal, J. C., Hopper, J. R.: GlobSed: Updated total sediment thickness in the world's oceans, Geochem. Geophy. Geosy., 20, 1756-1772, https://doi.org/10.1029/2018GC008115, 2019.

Tesauro, M., Audet, P., Kaban, M. K., Bürgmann, R., and Cloetingh, S.: The effective elastic thickness of the continental lithosphere: Comparison between rheological and inverse approaches, Geochem. Geophy. Geosy., 13, Q09001, https://doi.org/10.1029/2012GC004162, 2012.

Til'man, S. M., Belyy, V. F., Nikolayevskiy, A. A., and Shilo, N. A.: Tectonics of the northeast of the USSR: USSR Academy of Sciences, Siberian Branch, North East Interdisciplinary Sciences Research Institute (NEISRI): Transactions, 33, 80 p. (in Russian), 1969.

Turcotte, D. L., Schubert, G.: Geodynamics, 2nd ed.; Cambridge University Press: Cambridge, United Kingdom, 1982; pp. 123–131.

Wienecke, S., Braitenberg, C., Götze, H.-J.: A new analytical solution estimating the flexural rigidity in the Central Andes, Geophys. J. Int., 169, 789–794, https://doi.org/10.1111/j.1365-246X.2007.03396.x, 2007.

Wilson, D., Aster, R., West, M., Ni, J., Grand, S., Gao, W., Baldridge, W., Semken, S., and Patel, P.: Lithospheric structure of the Rio Grande rift, Nature, 433, 851-855, https://doi.org/10.1038/nature03297, 2005.

Zorin, Y. A., Pismenny, B. M., Novoselova, M. R., Turutanov, E. K.: Decompensative gravity anomalies, Geologia i Geofizika , 8, 104-108 (in Russian), 1985.

Zorin, Yu. A., Belichenko, V. G., Turutanov, E. Kh., Kozhevnikov, V. M., Ruzhentsev, S. V., Dergunov, A. B., Filippova, I. B., Tomurtogoo, O., Arvisbaatar, N., Bayasgalan, Ts., Biambaa, Ch., and Khosbayar, P.: The south Siberia-central Mongolia transect, Tectonophysics, 225, 361-378, https://doi.org/10.1016/0040-1951(93)90305-4, 1993.

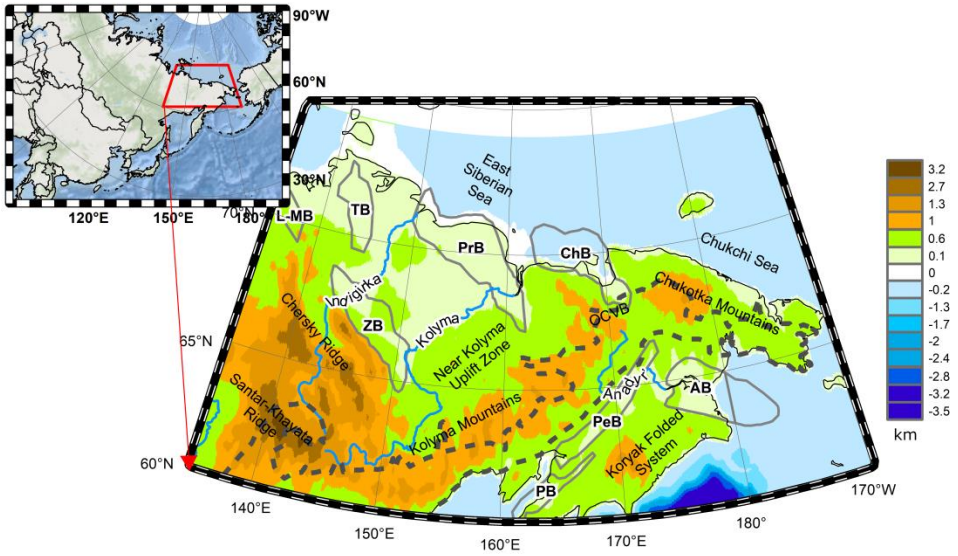

Figure 1 Topography and bathymetry of the study area. Dark grey contours represent positions of sedimentary basins. The basin captions are in bold. The dashed line indicates the OCVB continental borders. Here and in all subsequent maps the following abbreviations are used to denote the following sedimentary basins: L-MB – Laptev-Moma basin, ZB – Zyryanka basin, PrB – Primorsk basin, TB – Tastakh basin, ChB – Chauna basin, PeB – Penzhin basin, PB – Pustorets basin, AB – Anadyr basin.

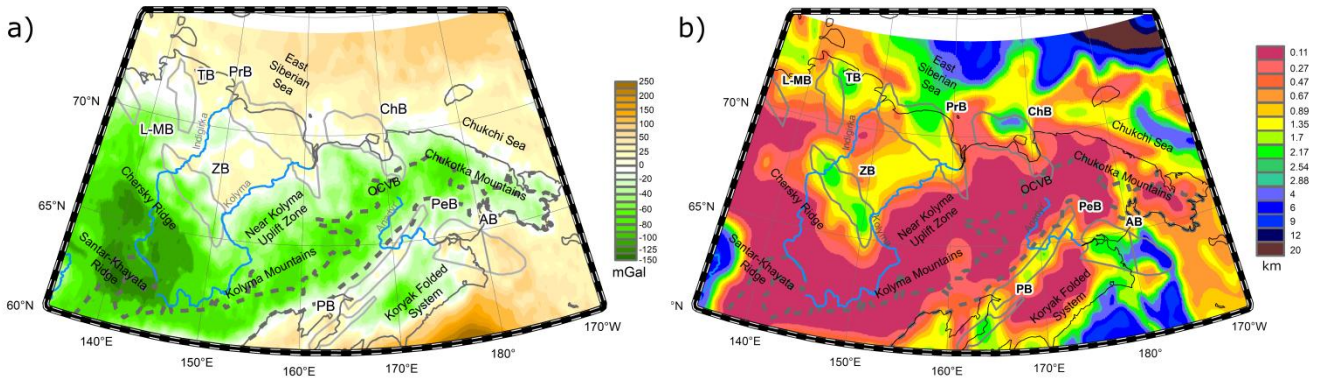

Figure 2 (a) Initial Bouguer gravity data. (b) Thickness of sediments according to the initial model.

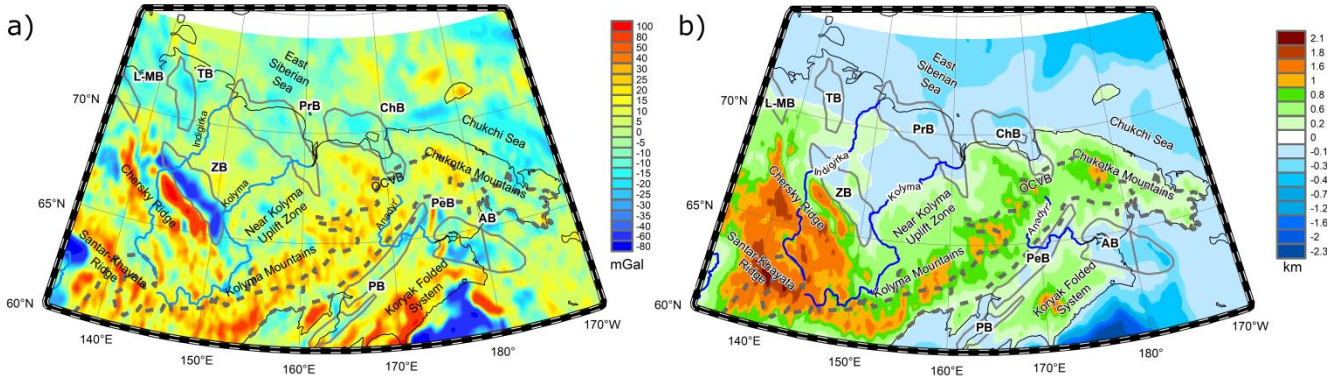

Figure 3 (a) Residual gravity anomalies. (b) Adjusted topography representing a unified surface load with the standard density of topography (2.67 g/cm^3, Eq. (2)).

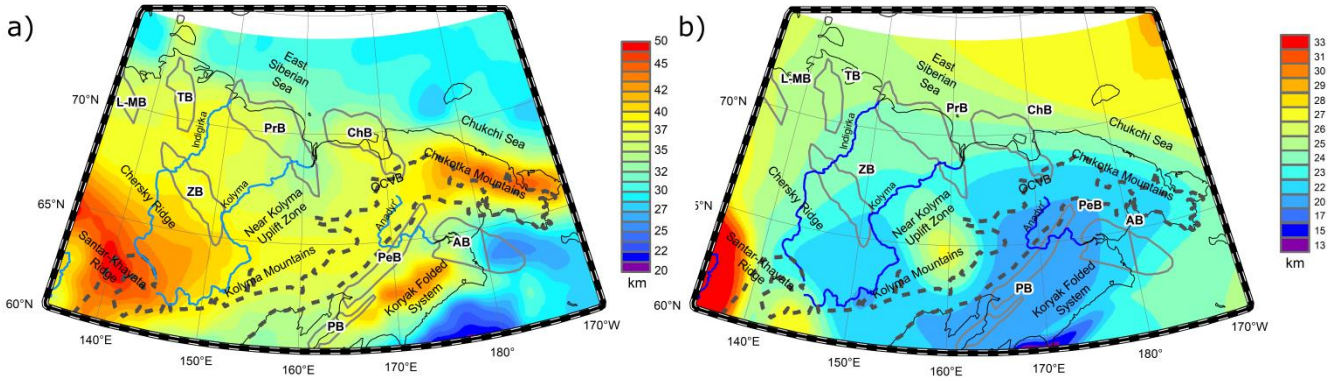

Figure 4 (a) Depth to the Moho from the sea level. (b) EET of the lithosphere.

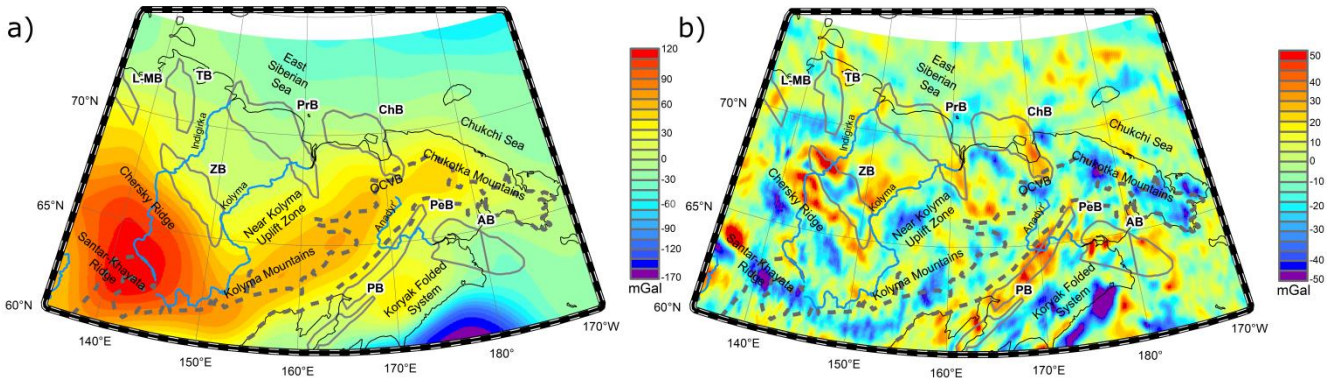

Figure 5 (a) Isostatic correction. (b) Residual isostatic gravity anomalies (also implying the the effect of the initial model of sediments).

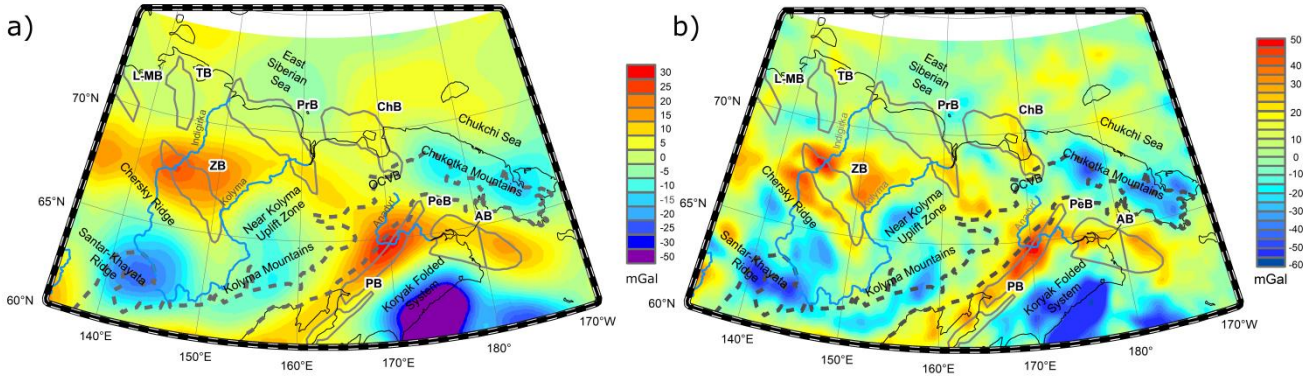

Figure 6. (a) Decompensative correction for the isostatic gravity anomalies. (b) Decompensative gravity anomalies.

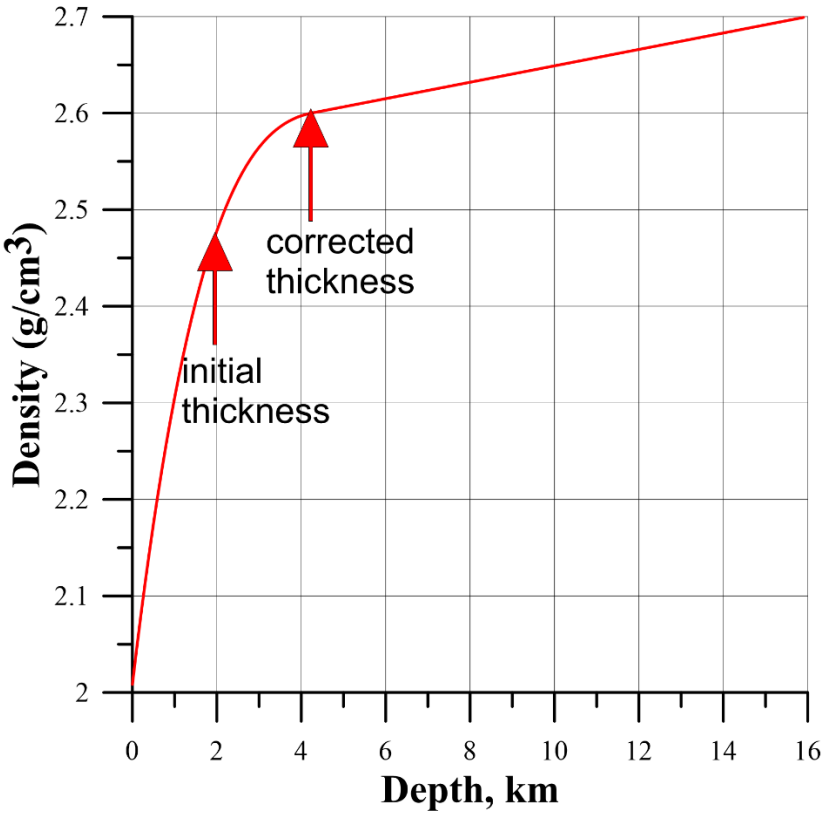

Figure 7. Illustration of the sedimentary thickness correction. This example corresponds to a negative decompensative anomaly.

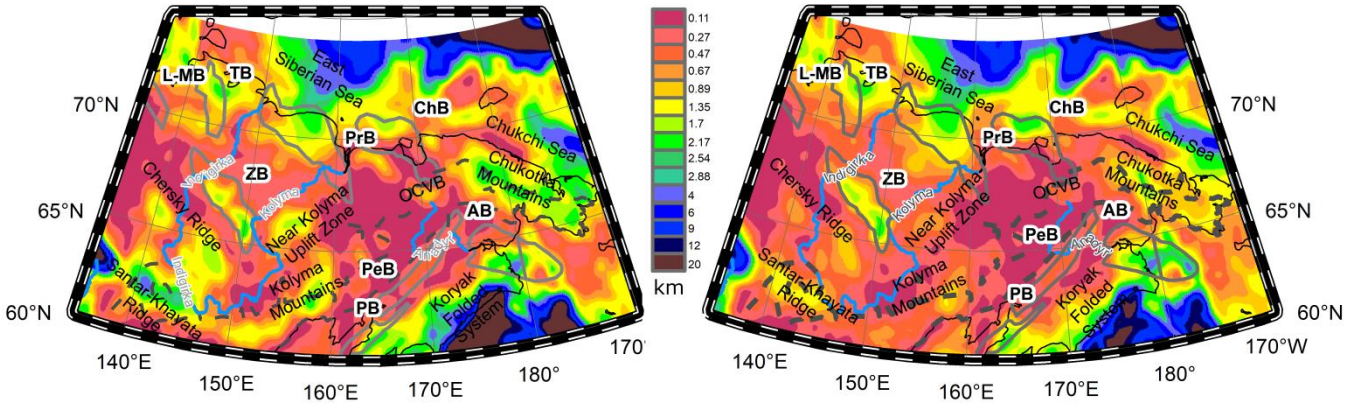

Figure 8. New model of sedimentary cover. (a) Model 1. (b) Model 2.

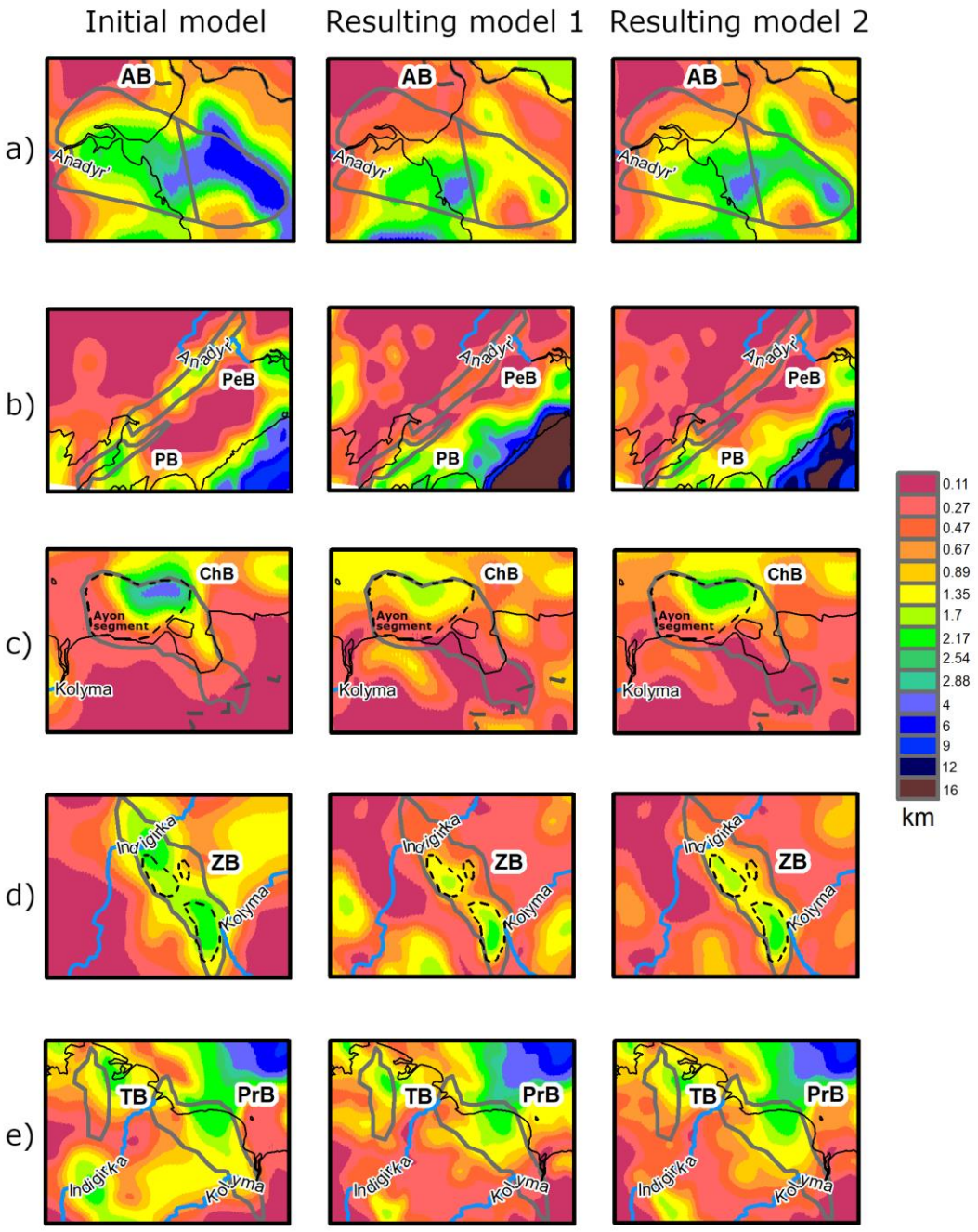

Figure 9. Comparison between the initial sedimentary model (left) and the new sedimentary cover models, 1 (center) and 2 (right) for several basins: Anadyr (a), Penzhin and Pustorets (b), Chauna (c), Zyryanka (d, dashed lines show the Lower Cretaceous coal-bearing zones), Primorsk and Tastakh (e).

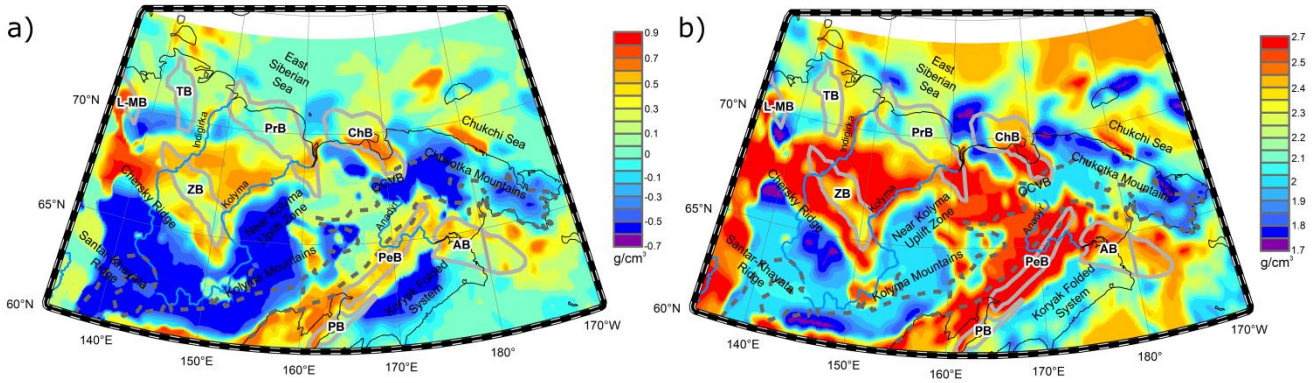

Figure 10. (a) Density correction. (b) Corrected density model (vertically averaged).

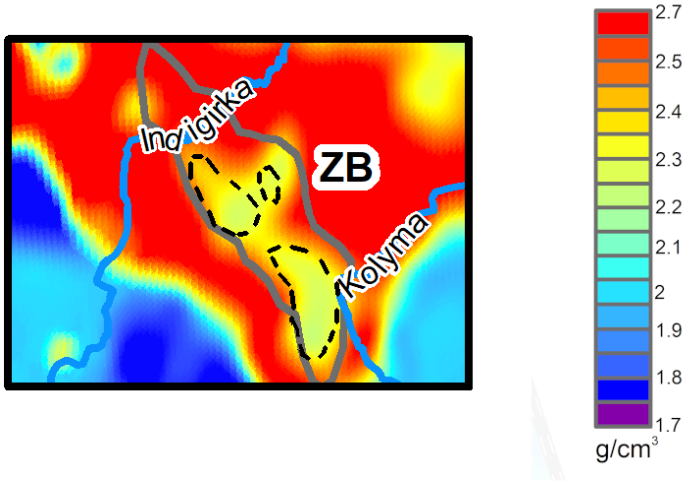

660 **Figure 11. New density model zoomed in on the Zyryanka basin. Dashed lines show the Lower Cretaceous coal-bearing zones.**